EPJ E
Soft Matter and Biological Physics
EPJ.org
your physics journal

Eur. Phys. J. E **29**, 311–318 (2009) DOI: 10.1140/epje/i2009-10490-x

Partial clustering prevents global crystallization in a binary 2D colloidal glass former

F. Ebert, G. Maret and P. Keim

EDP SCIENCES Società Italiana di Fisica Springer

Eur. Phys. J. E **29**, 311–318 (2009)
DOI 10.1140/epje/i2009-10490-x

THE EUROPEAN PHYSICAL JOURNAL E

Regular Article

Partial clustering prevents global crystallization in a binary 2D colloidal glass former

F. Ebert, G. Maret, and P. Keim[a]

Fachbereich für Physik, Universität Konstanz, D-78457 Konstanz, Germany

Received 27 April 2009 and Received in final form 9 June 2009
Published online: 11 July 2009 –

Abstract. A mixture of two types of super-paramagnetic colloidal particles with long-range dipolar interaction is confined by gravity to the flat interface of a hanging water droplet. The particles are observed by video microscopy and the dipolar interaction strength is controlled via an external magnetic field. The system is a model system to study the glass transition in 2D, and it exhibits *partial clustering* of the small particles (N. Hoffmann *et al.*, Phys. Rev. Lett. **97**, 078301 (2006)). This clustering is strongly dependent on the relative concentration ξ of big and small particles. However, changing the interaction strength Γ reveals that the clustering does not depend on the interaction strength. The *partial clustering* scenario is quantified using *Minkowski* functionals and partial structure factors. Evidence that partial clustering prevents global crystallization is discussed.

PACS. 82.70.Dd Colloids – 64.70.P- Glass transitions of specific systems

1 Influence of dimensionality on frustration

It is well known that the macroscopic behavior of crystalizing systems sensitively depends on dimensionality, as demonstrated by two examples: In 2D an intermediate phase exists between fluid and crystal, the *hexatic phase*, where the system has no translational order while the orientational correlation is still long range [1–3]. Such a two-step melting scenario is not known in 3D. The *Ising* model for ferromagnetics shows a phase transition for 2D and 3D but not for 1D [4]. For amorphous systems, however, it was found in experiments [5], simulations [6], and theory [7] that the glass transition phenomenology is very similar in 2D and 3D systems, both in dynamics and structure [5,8].

A subtle difference, the local density optimization in 2D and 3D, is the following: in 3D the local density optimized structure of four spheres is obviously a tetrahedron. However, it is not possible to completely cover space in 3D with tetrahedra, because the angle between two planes of a tetrahedron is not a submultiple of 360° [9]. The density optimized state with long-range order is realized by the *hexagonal closed-packed* structure or other variants of the *f.c.c.* stacking with packing fraction $\phi = \pi/\sqrt{18} \approx 74\%$. The dynamical arrest in 3D is expected to be enhanced by this geometrical frustration, because the system has to rearrange its local-density optimized structure to reach long-range order[1]. The local geometrical frustration scenario is different in 2D. There, the local-density optimized structure and densest long-range–ordered structure are identical, namely hexagonal. For the glass transition in 2D it is therefore expected that an increase of complexity is necessary to reach dynamical arrest without crystallization: in simulations an isotropic one-component 2D system has been observed undergoing dynamical arrest for an inter-particle potential that exhibits two length scales, a *Lennard-Jones-Gauss* potential with two minima [14]. Other simulations showed that systems of identical particles in 2D can vitrify if the mentioned local geometric frustration is created artificially via an anisotropic five-fold interaction potential [15]. Alternatively, the necessary complexity can be created by polydispersity as found in simulations [16].

A bi-disperse system in general is simple enough to crystallize as, *e.g.*, seen from the rich variety of binary crystal structures in an oppositely charged 3D Coulomb mixture [17]. In the system at hand, *partial clustering* prevents the homogenous distribution of particles and the system crystallizes locally into that crystal structure which is closest in relative concentration [8,18,19]. In this way the system effectively lowers its energy with a compromise between minimization of particle transport and minimization of potential energy. However, that means that the resulting structure is not in equilibrium, but in a frustrated glassy state. This competition of local stable

[a] e-mail: peter.keim@uni-konstanz.de

[1] It is found in 3D hard-sphere systems that this geometrical frustration *alone* is not sufficient to reach a glassy state as it cannot sufficiently suppress crystallization [10–12], and additionally polydispersity is needed [13].

crystal structures prevents the relaxation into an energetically equilibrated state, *i.e.* a large mono-crystal.

It was found that a binary mixture of magnetic dipoles is a good model system of a 2D glass former [5] as the dynamics and structure show characteristic glassy behavior: when the interaction strength Γ is increased, the system viscosity increases over several orders of magnitude while the global structure remains amorphous.

For all measured interaction strengths the system shows no long-range order as probed with bond order correlation functions [8]. However, on a local scale it reveals non-trivial ordering phenomena: *partial clustering* and *local crystallinity*.

Partial clustering [20,21] means that the small particles tend to form loose clusters while the big particles are homogeneously distributed. The heterogeneous concentration of small and big particles leads to a variety of local crystal structures when the system is supercooled making up the globally amorphous structure. This *local crystallinity* obviously plays a key role for the glass transition in this 2D colloidal system as it dominates the glassy structure [8]. Therefore, the phenomenon of *partial clustering* is indirectly responsible for the frustration towards the glassy state. In sect. 4 the details of the clustering scenario are explained. The dependence on the parameters accessible in experiment and the relation to *local crystallinity* [8] are discussed in sect. 5.

Firstly, the experimental setup is introduced. After a brief discussion about origin of *partial clustering*, a morphological analysis using *Minkowski* measures is presented to characterize and quantify the effect. Finally, the dependence on relevant parameters like the average relative concentration ξ and the interaction strength Γ will be discussed using *Euler* characteristics and the partial static structure factors.

2 Experimental setup

The detailed experimental setup is explained in [22]. It consists of a mixture of two different kinds of spherical and super-paramagnetic colloidal particles (species A: diameter $d_A = 4.5\,\mu$m, susceptibility $\chi_A = 7.4 \cdot 10^{-11}\,\mathrm{A\,m^2/T}$, density $\rho_A = 1.5\,\mathrm{g/cm^3}$ and species B: $d_B = 2.8\,\mu$m, $\chi_B = 6.6 \cdot 10^{-12}\,\mathrm{A\,m^2/T}$, $\rho_B = 1.3\,\mathrm{g/cm^3}$) which are confined by gravity to a water/air interface. This interface is formed by a water drop suspended by surface tension in a top sealed cylindrical hole (6 mm diameter, 1 mm depth) of a glass plate as sketched in fig. 1. A magnetic field $\mathbf{H}$ is applied perpendicular to the water/air interface inducing a magnetic moment $\mathbf{M} = \chi\mathbf{H}$ in each particle leading to a repulsive dipole-dipole pair interaction. Counterpart of the potential energy is thermal energy which generates *Brownian* motion. Thus the dimensionless interaction strength Γ is defined by the ratio of the potential *versus* thermal energy

$$\Gamma = \frac{E_{\mathrm{magn}}}{k_B T} \propto \frac{1}{T_{\mathrm{sys}}} = \frac{\mu_0}{4\pi} \cdot \frac{\mathbf{H}^2 \cdot (\pi\rho)^{3/2}}{k_B T} (\xi \cdot \chi_B + (1-\xi)\chi_A)^2. \quad (1)$$

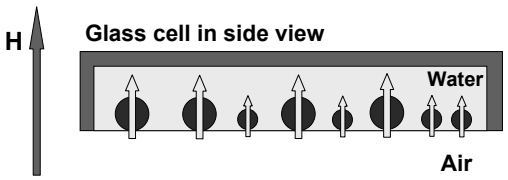

Fig. 1. Super-paramagnetic colloidal particles confined at a water/air interface due to gravity. The curvature of the interface is actively controlled to be completely flat; therefore the system is considered to be ideal two-dimensional. A magnetic field $\mathbf{H}$ perpendicular to the interface induces a magnetic moment $\mathbf{m}$ in each bead leading to a repulsive dipolar interaction.

Here, $\xi = N_B/(N_A + N_B)$ is the relative concentration of small species with N_A big and N_B small particles and ρ is the area density of all particles. The average distance of neighboring big particles is given by $l_A = 1/\sqrt{\rho}_A$. The interaction strength can be externally controlled by means of the magnetic field $\mathbf{H}$. Γ can be interpreted as an inverse temperature and controls the behavior of the system.

The ensemble of particles is visualized with video microscopy from below and the signal of a CCD 8-Bit grayscale camera is analyzed on a computer. The field of view has a size of $1170 \times 870\,\mu\mathrm{m}^2$ containing typically $3 \cdot 10^3$ particles, whereas the whole sample contains about up to 10^5 particles. Standard image processing is performed to get size, number and positions of the colloids. A computer-controlled syringe driven by a micro-stage controls the volume of the droplet to get a completely flat surface. The inclination is controlled actively by micro-stages with a resolution of $\alpha \approx 1\,\mu$rad. After several weeks of adjusting and equilibration, this provides best equilibrium conditions for long-time stability. Trajectories for all particles in the field of view can be recorded over several days providing the whole phase space information.

3 Origin of partial clustering

The origin of the clustering phenomenon lies in the negative *nonadditivity* of the binary dipolar pair potential [20, 21]. It is not expected in positive nonadditive mixtures like colloid-polymer mixtures or additive mixtures like hard spheres. In binary mixtures with additive hard potentials in 2D, phase separation was found using *Monte Carlo* simulations [23]. In addition to the negative nonadditivity, the relation $v_{BB} < v_{AB} < v_{AA}$ of the pair potentials has to be fulfilled [20,21]. Why this leads to partial clustering can be understood as follows: The negative nonadditivity prevents macro-phase separation as the negativity of the nonadditivity parameter $\Delta = 2\sigma_{AB} - (\sigma_{AA} + \sigma_{BB})$ means that particles are effectively smaller in a mixed state ($\sigma_{ij} = \int_0^\infty \mathrm{d}r\{1 - \exp[-v_{ij}(r)/k_B T]\}$ are the *Barker-Henderson* effective hard-core diameters). Thus, a mixed configuration is preferred this way. Additionally, the inequality $v_{AB} < v_{AA}$ energetically favors direct neighbor connections between different species instead of big particles being neighbors. In competition to this, the inequality $v_{BB} < v_{AB}$ favors the neighboring of small particles. The

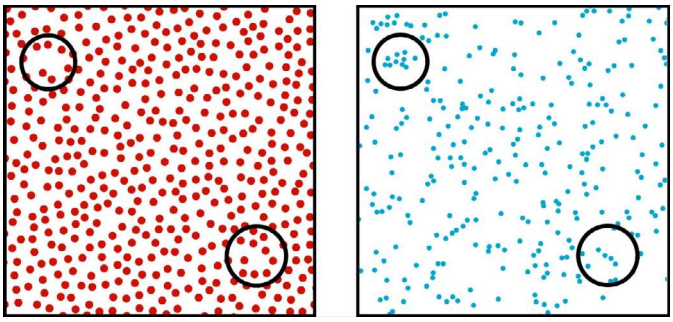

Fig. 2. Snapshot of a particle configuration ($\Gamma = 5$, relative concentration $\xi = 41\%$) where big (left) and small (right) particles are displayed separately. The clusters of small particles (right) fit in the voids formed by the big particles (left) as highlighted by circles for two examples.

best compromise is achieved in the partial clustered arrangement: neighboring small particles that are located in the voids of big particles.

The genuineness of the effect was demonstrated by a comparison of computer simulation, theory and experiment [20]. There, statistical evidence for the occurrence of *partial clustering* is provided by the static structure factor. The structure factor $S_{AA}(k)$ has the characteristic shape of a one-component fluid. In contrast, the structure factor of the small particles $S_{BB}(k)$ has a dominant prepeak at small wave vectors which is statistical evidence for an inherent length scale much larger than the typical distance between two neighboring small particles: it is the length scale of the clusters.

The prepeak provides statistical evidence of an inherent length scale in the small-particle configurations. However, the structure factors do not reveal all details of the phenomenon. For example, the voids seen in the big particle configurations (see fig. 2) are not reflected directly in the features of the partial structure factors. To further elucidate the scenario, the effect is now investigated from a morphological point of view using *Minkowski* measures as this provides additional quantitative insight.

4 Morphological analysis

For low interaction strengths Γ the system is an equilibrated fluid as seen from the purely diffusive behavior [5]. Assuming that entropy is maximized, it might be intuitively expected that particles form an arbitrarily mixed state where small and big particles are evenly distributed. However, already the inspection of a single snapshot reveals that this is not the case, and the scenario turns out to be more subtle. How the system appears in equilibrium at low interaction strengths Γ is demonstrated in fig. 2. There, a configuration with relative concentration $\xi = 41\%$ at $\Gamma = 5$ is separately plotted for big (left) and small (right) particles. Big particles are distributed more evenly while the small particles form loose clusters. Configurations of big and small particles are related because small-particle clusters are able to push away the big particles and form voids in the big-particle configuration. This connection becomes obvious in the highlighted regions where two big clusters of small particles create two voids in the big-particle configuration. This visual impression of the configurational morphology will be quantified in detail after a brief introduction of the used tools, the *Minkowski* measures.

Minkowski functionals provide morphological measures for characterization of size, shape, and connectivity of spatial patterns in d dimensions [24]. These functionals turned out to be an appropriate tool to quantify clustering substructures in astronomy, *e.g.* from galaxies [25]. They also give insight into the morphology of random interfaces in microemulsions [26].

The scalar *Minkowski* valuations V applied to patterns P and Q in *Euclidian* space are defined by three types of covariances [25]:

1) Invariance to motion.
2) Additivity: $V(P \bigcup Q) = V(P) + V(Q) - V(P \bigcap Q)$.
3) Continuity: continuous change for slight distortions in pattern P.

It is guaranteed by the theorem of *Hadwiger* that in d dimensions there are exactly $d+1$ morphological measures V that are linearly independent [24]. For $d = 2$, the three functionals have intuitive correspondences[2]: The *surface area*, the *circumference* of the surface area, and the *Euler characteristic* χ.

In two dimensions the *Euler characteristic* χ for a pattern P is defined as

$$\chi = S - H, \tag{2}$$

where S is the number of connected areas and H the number of holes.

Morphological information can also be obtained from particle configurations. As configurations only consist of a set of coordinates, a cover disc with radius R is placed on each coordinate to construct a pattern that can be evaluated.

The *Minkowski* measures are then determined for different cover radii R, leading to a characteristic curve for a given configuration, explained in the following (for better understanding, follow the curves in fig. 3).

The first *Minkowski* measure (disc area normalized to total area) increases from 0% to 100% for increasing radius R with a decreasing slope when discs start to overlap. The second *Minkowski* measure (circumference) increases with cover radius R, reaches a maximum, and then decays to zero when all holes are overlapped. The third *Minkowski* measure (*Euler characteristic*) is very subtle and describes the connection of cover discs and the formation of holes. It allows the most detailed interpretation of a given configuration.

A typical devolution of an *Euler characteristic* χ/N with N particles can be divided in three characteristic parts for continuously increasing cover disc radius R:

1) For small R the curve is constant at $\chi/N = 1$ (normalized to the number of particles N). Discs are not

[2] For $d = 3$ a common set of functionals correspond to: volume, area, integral mean curvature, and *Euler characteristic*.

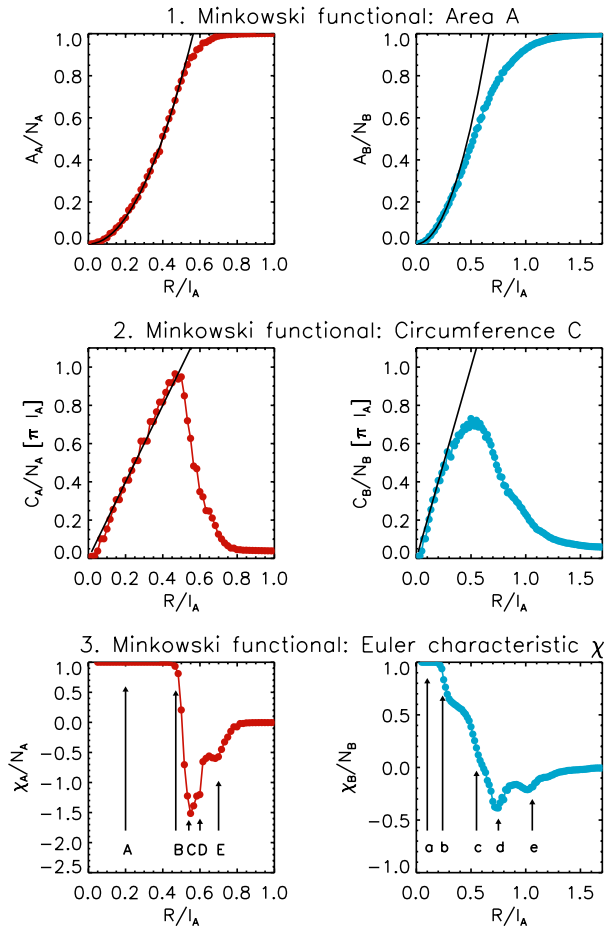

Fig. 3. The three *"Minkowski"* measures in 2D ("area", "circumference", and "Euler characteristic") are shown for a sample with $\xi = 42\%$ at $\Gamma = 662$, separately for big (left graphs) and small particles (right graphs). Configurations were decorated with discs and the *"Minkowski"* measures are calculated in dependence on their radius R/l_A. The solid lines correspond to the *"Minkowski"* measures of a single cover disc. Marks A-E and a-e in the bottom graphs correspond to radii of interest, and an example of a representative configuration at these labels is displayed in fig. 4. The features of all measures confirm the clustering scenario.

touching and thus S is equal to the number of particles. No holes are present. As χ is normalized with the number of points, the *Euler characteristic* amounts to $\chi/N = 1$.

2) With increasing R the curve drops and χ/N can become negative when cover discs are large enough to overlap and holes are formed. Therefore, the number of connected areas S decreases and holes are forming which further decreases χ/N. The minimum is reached when discs are connected to a percolating network and the maximum number of holes has formed.
3) For large R the curve starts to raise again because the holes are collapsing until the whole plane is covered with overlapping discs and $\chi/N \to 0$ for $R \to \infty$.

This qualitative behavior is typical for configurations in 2D. However, the individual morphological information is obtained from specific features in the three regions as the onset of the fall and rise, characteristic kinks or plateaus, and the slope of the fall and rise. The *Minkowski* measures in dependence on an increasing cover disc provide a characteristic morphological "fingerprint" of configurations and therefore statistical evidence of the clustering scenario, complementary to structure factors [20,21]. The statistical noise of the curves is remarkably small compared to that of structure factors as the whole statistical information of a configuration is contained in *every* data point. Thus, even small features in the curves are true evidence for morphological particularities.

All three *Minkowski* measures in 2D, *area*, *circumference*, and *Euler characteristic*, are averaged over 100 configurations for a given temperature and no time dependence was found during this period of about half an hour. The curves are plotted separately for both species in fig. 3 in dependence on the cover disc radius. Corresponding snapshots are displayed in fig. 4 to illustrate characteristic radii as indicated. The used sample was strongly supercooled ($\Gamma = 662$, $\xi = 42\%$), *i.e.* it was not in equilibrium. However, the features found at these high interaction strengths are the same as for low Γ, where the sample is in equilibrium. The high interaction strength is used here, as the discussed features become clearer, but it is assumed in the following that the conclusions on clustering are also valid for low interaction strengths Γ. This assumption will be justified when the dependence on the interaction strength is discussed in sect. 5.

First Minkowski measure: Area

The upper graphs of fig. 3 show the area per particle in dependence on the cover radius R/l_A. The covered area starts at zero and is increased continuously to 100% when the discs completely overlap the area. The solid line in both plots indicates the area fraction covered by nontouching free discs. The deviation of the first *Minkowski* measure from that line shows how homogeneous a configuration is. A clear difference is found between particle species: The big particles follow this reference line up to $\approx 80\%$. This is close to the maximum possible value for hard discs between 84% and 90.7% for *random close packing* and *hexagonal close packing*, respectively [7,27,28]. Therefore, the big-particle configurations are very homogeneously distributed. However, the small-particle curve deviates from the free-disc reference much earlier at $\approx 40\%$, indicating that small particles are much less evenly spread, *i.e.* they form clusters.

Second Minkowski measure: Circumference

The middle graphs show how the circumference depends on the radius. The black reference line corresponds to a free expanding circle. The measure of the big particles follows this reference line up to $R/l_A \approx 0.5$ and then sharply decreases. Again, this is due to the homogeneous distribution of the big particles. Their cover discs can expand

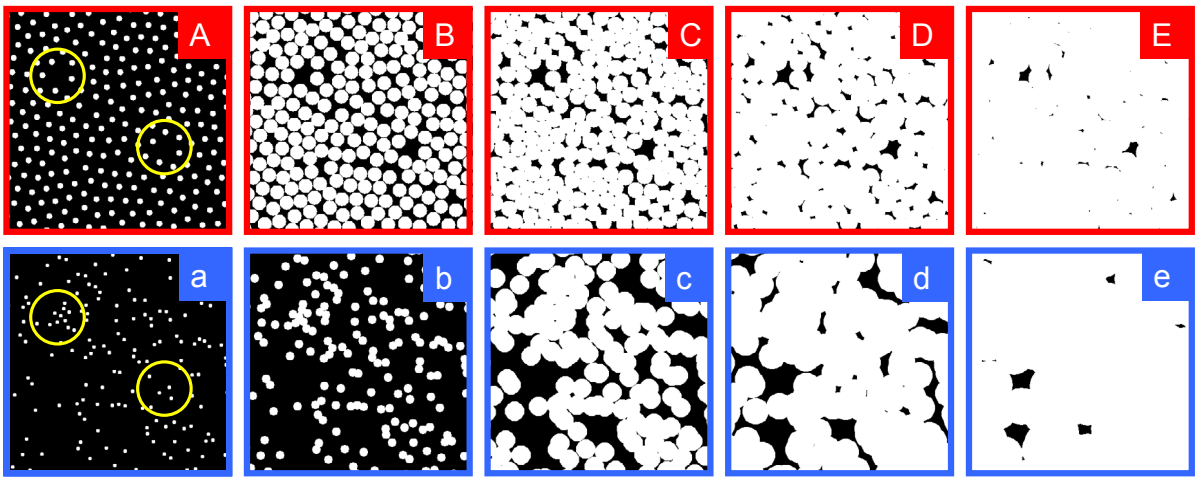

Fig. 4. The same section ($375 \times 375\,\mu\mathrm{m}^2$) of a single particle configuration with cover discs is shown several times in the pictographs A-E and a-e with increasing radius. Pictures correspond to certain radii of interest marked by arrows in the corresponding graphs of the "Euler characteristic" in fig. 3. In the first (second) row, just the big (small) particles of this particular configuration are shown. Voids in the big particle configurations are filled with clusters of small particles (examples are highlighted with circles in pictograph "A" and "a", respectively). Configurations were obtained from a sample with $\xi = 42\%$ at $\Gamma = 662$.

freely up to the maximum possible value of $R_{\max}/l_A = 1/2$ for square order. The measure of the small particles deviates much earlier and less steeply as their particle density is very heterogeneous, *i.e.* clustered.

Third Minkowski measure: Euler characteristic

The most detailed information on morphology is obtained from the *Euler characteristic*. It exhibits many features related to characteristic structures of the investigated configurations. For better understanding of the features described in the following, fig. 4 shows snapshots of a typical section in the used configuration for specific cover-radii. The notation A-E for the big particles and a-e for the small ones is used in both figs. 3 and 4. In fig. 4a and 4A two clusters are highlighted. Firstly, we consider only the big particles. The *Euler characteristic* χ_A per particle is 1 as the expanding discs are not touching for small radii (mark A). Again, this continues up to a value close to $R/l_A \approx 0.5$. The characteristic deviation of all three measures at this same radius states the homogeneity of the big-particle distribution. Then, discs touch and χ_A/N_A decreases rapidly because surfaces are connecting and holes are forming (mark B). The minimum is reached at mark C, and the *Euler characteristic* immediately raises because the smallest holes between the triangular close-packed regions collapse as seen in the comparison of figs. 4C and 4D. The next holes to collapse are those where one small isolated particle is located. Therefore, a little kink is visible at mark D since these one-particle holes are a little larger than the holes decaying at mark C and therefore "survive" a little longer. When they collapse, the *Euler characteristic* increases rapidly to a pronounced plateau. Note that this plateau is the only statistical evidence for the voids in the big particle configuration made up by the clusters: these voids are large and thus they "survive" for a long "time" resulting in that plateau. These voids are not detectable with the other *Minkowski* measures or the static structure factor of the big particles [20,21]. Finally, they start to decay at mark E, but not suddenly, which shows that they have a distribution in size.

The *Euler characteristic* of the small particles shows the complementary picture: Starting with low values of R/l_A the characteristic is $\chi_B/N_B = 1$ for free disc expansion. The first drop at mark b occurs at much lower values than for the big particles because small particles in clusters connect. The subsequent shoulder right next to mark b confirms the clustering: small particles inside a cluster are now connected, and it needs some further increase of disc radius until the clusters themselves start connecting. A small second shoulder at mark c originates from the isolated particles that are not arranged in clusters. They are the last particles incorporated until all discs form a percolating network at the minimum at mark d. The increase of χ_B/N_B shows how the holes are closing. While the increase in the *Euler characteristics* of the big particles has a plateau at mark E, the small particles have a clear dip at mark e. This reveals information on the shape of the clusters: The voids in the big particle positions are compact in shape stopping the increase of the *Euler characteristic* before mark E. In contrast, the small particles arrange in chain-like clusters. When the voids between these structures close, they decay into several sub-holes causing the characteristic to decrease again. In fact, the big particles also cause a little dip at their plateau for the voids can sometimes also decay into sub-holes. However, this dip is much smaller than for the small ones.

Most features are also visible in the *Euler characteristic* obtained from *Brownian dynamics* simulation [20]. There, the same qualitative behavior is found but the smaller features are "washed out" because the used interaction strengths were much lower, as discussed in the

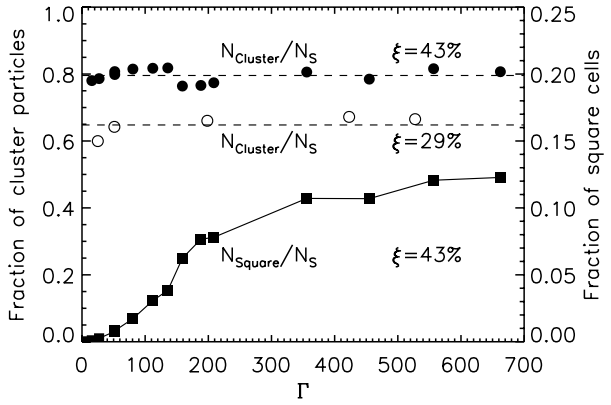

Fig. 5. Fraction of small particles (relative to all small particles N_S, left axis) that are arranged in clusters. This fraction is independent of Γ but dependent on the relative concentration ξ. The dashed lines correspond to the average fractions over all interaction strengths Γ. Solid squares represent the fraction of small particles (relative to all small particles N_S, right axis) that are arranged in square symmetry as evaluated in [8].

following section. Further, the variation of the relative concentration ξ and the subsequent dependence of the features in the *Euler characteristic* will confirm the interpretation of the scenario.

5 Dependence of clusters on interaction strength and relative concentration

In order to demonstrate the connection between clustered equilibrated fluid and supercooled local crystalline structure, the dependence of partial clustering on the interaction strength Γ and on the average relative concentration ξ is now discussed.

In fig. 5 the fraction of small particles arranged in clusters is plotted *versus* interaction parameter Γ for two different relative concentrations ξ. A small particle is characterized as "cluster-particle", when the closest neighbor is also a small particle. This simple criteria implies that the smallest possible cluster consists of two close small particles surrounded by a cage of big ones. In the graph of fig. 5 for $\xi \approx 43\%$ it is found that a high fraction of $\approx 80\%$ of all small particles is arranged in clusters. Even for a lower relative concentration $\xi \approx 29\%$, still $\approx 65\%$ are arranged in clusters. Note that the fraction of small particles in both samples is smaller than that of the big particles as $\xi < 0.5$. Therefore, every small particle could have enough possibilities to arrange far away from the next small particle which is obviously not the case. For an arbitrary distribution of the small particles over the number of possible sites (which is equal to the number of big particles) a fraction of 40% is expected for a relative concentration $\xi = 29\%$ and a fraction of 55% for a relative concentration $\xi = 43\%$[3]. The fact that these expected values are significantly lower than the actually measured ones additionally confirms that small particles effectively attract each other and therefore cluster.

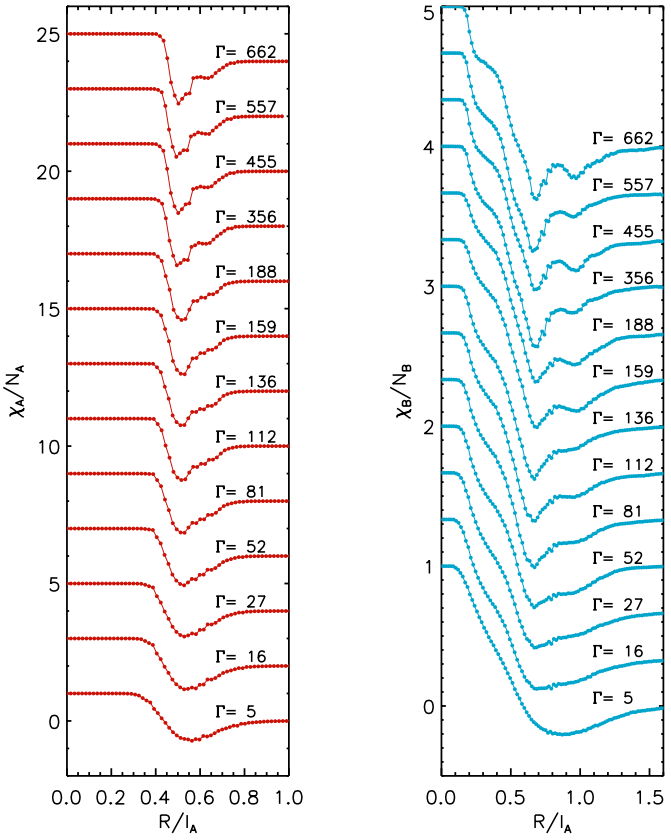

Fig. 6. "Euler characteristics" of big (left) and small (right) particles for different interaction strengths Γ. Characteristic features are visible for the lowest Γ and become clearer with increasing Γ. The relative concentration was $\xi \approx 43\%$. Curves are shifted for clarity.

The main result from fig. 5 for the structure of this colloidal glass former is that the fraction of cluster-particles is independent of the interaction parameter Γ, in contrast to local crystallinity which strongly increases upon supercooling: Clusters do not vanish although the local structure is dominated by local crystallinity for strong supercooling [8]. This is demonstrated for the example of square order in the same fig. 5 (for details, see [8]).

The local relative *concentration* is frozen in. Small particles are not redistributed to match an equilibrium crystal structure which would reduce the number of cluster-particles (*e.g.* in square order). In fact, the independence of the clustering from Γ shows that the opposite is the case: The clusters force the local structure into that crystalline order which matches best with the local relative concentration. In this way, local crystallinity is established without long-range order [8] as it inherits the clustered distribution of the small particles.

This behavior is confirmed by the graphs of fig. 6. The *Euler characteristics* for both species are plotted over a wide range of the interaction strength Γ, from fluid ($\Gamma = 5$) to the strongly supercooled state ($\Gamma = 662$):

[3] A simple simulation is performed where N_A sites are randomly occupied with small particles, and the same analysis to determine the number of cluster-particles is applied.

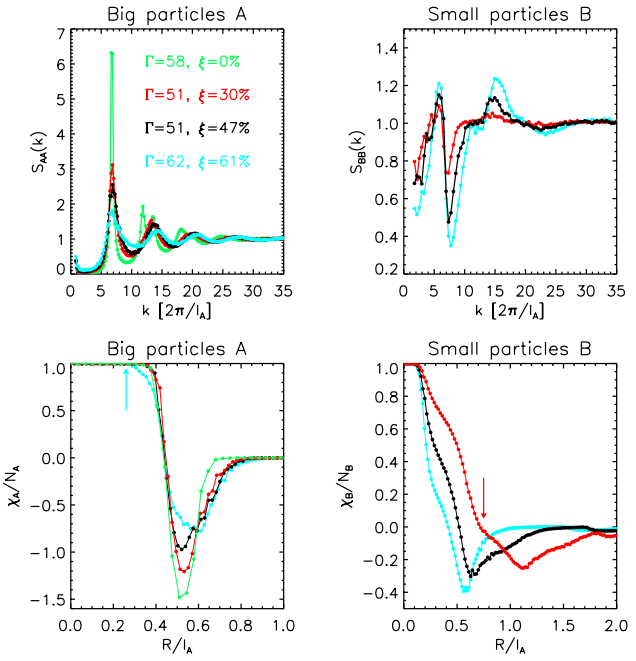

Fig. 7. (Colour on-line) Static structure factors and *"Euler characteristics"* of samples with comparable interaction strength Γ but different relative concentration ξ. Indicated values for Γ and ξ are valid for all graphs. Upper graphs: Static structure factors for big (left) and small particles (right). With increasing relative concentration of small particles the features of $S_{BB}(k)$ gain more contrast, and peaks in the $S_{AA}(k)$ are shifted slightly towards higher k-values. Lower graphs: *"Euler characteristics"* for big (left) and small particles (right). For decreasing ξ the minimum in χ_B/N_B is shifted towards larger radii R. The weight of the features changes, see, *e.g.*, the last shoulder in the drop in χ_B/N_B (red arrow, right plot). This shoulder results from the incorporation of isolated small particles into the network (see fig. 3) and is only visible for the lowest relative concentration $\xi = 30\%$ (red curve) at this interaction strength Γ. The blue arrow in the bottom left plot marks the onset of the inter-particle connection of the big particles for the sample with highest relative concentration $\xi = 61\%$. The onset is shifted to a lower value R compared to the other curves.

the curves change continuously. The main clustering features as discussed in fig. 4 are visible for all values of Γ, they just become sharper with increasing the interaction strength. The smallest features like the kink at mark D in fig. 3 are smeared out for low Γ but the plateaus and shoulders characterizing the *partial clustering* are qualitatively independent of Γ.

In fig. 7 the dependence of the local structure on the relative concentration ξ is shown using structure factors and *Euler characteristics*. There, samples with comparable interaction strengths Γ but different relative concentrations ξ are compared. Adding small particles is shifting the peaks of the structure factor $S_{AA}(k)$ towards higher k-values. This can be understood by the clustering effect: Small particles form clusters and push the big particles closer together resulting in a shift of the main peak. This shift is small for the used parameters. However, confirmation of this interpretation is found in [21] where *Liquid integral equation theory* shows the same result unambiguously. There, parameters were used that are not accessible in the experiment (different ratios of the magnetic moments χ_B/χ_A). The contrast in $S_{BB}(k)$ is increased for higher relative concentrations ξ which is also in agreement with theory [21].

The *Euler characteristics* for the same samples, shown in the lower graphs of fig. 7, confirm this interpretation. The drop in the χ_A/N_A (bottom left) becomes deeper when less small particles are present. Then, the distances between big particles are less distributed due to fewer clusters. The increase becomes steeper for the same reason: clusters of small particles cause larger voids collapsing at higher cover disc radii. It is remarkable that the onset of the steep drop is earlier for high relative concentrations ($\xi = 61\%$, blue curve) as indicated by the blue arrow. Again, this is caused by the small-particle clusters that push together the big particles.

A strong dependence is found in the *Euler characteristics* of the small particles: the onset of the first drop is independent of the relative concentration indicating that the local density of particles in clusters is not affected (unlike that of big ones). What significantly changes is the depth of the first drop. The smaller the particles, the deeper the drop, because more small particles are arranged in clusters. The last shoulder, before the *Euler characteristic* reaches its minimum (marked by red arrow), refers to the isolated particles (see sect. 4). Therefore, at these interaction strengths this shoulder is only visible for the sample with the lowest relative concentration $\xi = 30\%$ (red curve) which has the most isolated particles (compare also with fig. 5).

The systematic dependence of *Euler characteristics* and static structure factors on the relative concentration ξ confirms the interpretation of *partial clustering* of sect. 4. However, the main result of this section is that the principle occurrence of the effect is independent of the interaction strength: The clustering in equilibrium at low interaction strengths is therefore responsible for the variety of local crystallinity at strong supercooling suppressing long-range order [8].

6 Conclusions

On a local scale the system reveals the nontrivial ordering phenomenon of *partial clustering*: the small particles tend to form loose clusters while the big particles are homogeneously distributed. The origin of this effect is traced back to the negative *nonadditivity* of the dipolar pair potential. The detailed scenario is quantified using *Minkowski* functionals applied to experimentally obtained configurations. Changing the interaction strength Γ reveals that the principle scenario does not qualitatively depend on the interaction strength, and, as a consequence, the local relative concentration is simply "frozen" in. However, the strength of the effect increases with the relative concentration ξ.

The clustering effect together with the missing ability of the system to reorganize fast enough into an equilibrated state (*i.e.* extended crystal structure [8,18,19]) is crucial to understand the glass forming behavior of this system: The *partial clustering* leads locally to a heterogeneous relative concentration ξ which then leads for increasing interaction strengths Γ to *local crystallinity* [8] without long-range order. It provides the necessary complexity for glassy frustration in this 2D system and prevents solidification into the energetically preferred crystalline or poly-crystalline morphologies [18,19].

This work was supported by the Deutsche Forschungsgemeinschaft SFB 513 project B6, SFB TR 6 project C2 and C4 and the International Research and Training Group "Soft Condensed Matter of Model Systems" project A7. We thank P. Dillmann for fruitful discussion and experimental contributions.

References

1. B.I. Halperin, D.R. Nelson, Phys. Rev. Lett. **41**, 121 (1978).
2. K. Zahn, G. Maret, Phys. Rev. Lett. **85**, 3656 (2000).
3. P. Keim, G. Maret, H.H. von Grünberg, Phys. Rev. E **75**, 031402 (2007).
4. L. Onsager, Phys. Rev. **65**, 117 (1944).
5. H. König, R. Hund, K. Zahn, G. Maret, Eur. Phys. J. E **18**, 287 (2005).
6. D. Perera, P. Harrowell, Phys. Rev. E **59**, 5721 (1999).
7. M. Bayer, J. Brader, F. Ebert, M. Fuchs, E. Lange, G. Maret, R. Schilling, M. Sperl, J. Wittmer, Phys. Rev. E **76**, 011508 (2007).
8. F. Ebert, P. Keim, G. Maret, Eur. Phys. J. E **26**, 161 (2008).
9. J.H. Conway, S. Torquato, Proc. Natl. Acad. Sci. U.S.A. **103**, 10612 (2006).
10. H.J. Schöpe, G. Bryant, W. van Megen, Phys. Rev. Lett. **96**, 175701 (2006).
11. M.D. Rintoul S. Torquato, Phys. Rev. Lett. **77**, 4198 (1996).
12. S.R. Williams, I.K. Snook, W. van Megen, Phys. Rev. E **64**, 021506 (2001).
13. P.N. Pusey, J. Phys.: Condens. Matter **20**, 494202 (2008).
14. T. Mizuguchi, T. Odagaki, M. Umezaki, T. Koumyou, J. Matsui, in *Complex Systems*, edited by M. Tokuyama, I. Oppenheim, H. Nishiyama, *AIP Conf. Proc.*, Vol. **982** (2008) p. 234.
15. H. Shintani, H. Tanaka, Nature Physics **2**, 200 (2006).
16. T. Kawasaki, T. Araki, H. Tanaka, Phys. Rev. Lett. **99**, 215701 (2007).
17. M. Leunissen, C. Christova, A. Hynninen, C. Royall, A. Campbell, A. Imhof, M. Dijkstra, R. van Roij, A. van Blaaderen, Nature **437**, 235 (2005).
18. L. Assoud, R. Messina, H. Löwen, EPL **80**, 48001 (2007).
19. J. Fornleitner, F. Lo Verso, G. Kahl, C.N. Likos, Soft Matter **4**, 480 (2008).
20. N. Hoffmann, F. Ebert, C. Likos, H. Löwen, G. Maret, Phys. Rev. Lett. **97**, 078301 (2006).
21. N. Hoffmann, C. Likos, H. Löwen, J. Phys.: Condens. Matter **18**, 10193 (2006).
22. F. Ebert, P. Dillmann, G. Maret, P. Keim, arXiv:0903.2808 (2009).
23. A. Buhot, W. Krauth, Phys. Rev. E **59**, 2939 (1999).
24. H. Hadwiger, *Vorlesungen über Inhalt, Oberfläche und Isoperimetrie* (Springer-Verlag, Berlin, 1957).
25. C. Beisbart, R. Valdarnini, T. Buchert, Astron. Astrophys. **379**, 412 (2001).
26. C.N. Likos, K.R. Mecke, H. Wagner, J. Chem. Phys. **102**, 9350 (1995).
27. J. Berryman, Phys. Rev. A **27**, 1053 (1983).
28. T.S. Majmudar, M. Sperl, S. Luding, R.P. Behringer, Phys. Rev. Lett. **98**, 058001 (2007).